Numerical simulation study on the heat dissipation characteristics of an air-cooled radiator

Kai Yan*, Feng Li, Jing Ren

CRRC Dalian Locomotive Research Institute Co., Ltd, Dalian, 116000 Liaoning, China

Abstract: This article conducts numerical simulation calculations on the heat dissipation characteristics of an air-cooled radiator. The results show that under natural heat dissipation conditions, the maximum temperature of air-cooled radiators with flat heat dissipation covers decreases by 9.6% compared to radiators without heat dissipation covers, and the maximum temperature of air-cooled radiators with array raised heat dissipation covers decreases by 9.9%; Under forced air cooling conditions, the maximum temperature of an air-cooled radiator with a flat heat dissipation cover decreases by 12.7%, while the maximum temperature of an air-cooled radiator with an array raised heat dissipation cover decreases by 13.3%.

1 Introduction

Air cooled radiators are widely used in various engineering equipment due to their simple structure and high reliability. However, compared to methods such as water cooling and evaporative cooling, the heat transfer coefficient of air cooling is lower. For air-cooled radiators, researchers and engineers improve their heat transfer coefficient and heat transfer performance by improving their fins and other methods [1-5].

Electric motors are an important engineering equipment, and their heat dissipation is mainly achieved through natural cooling or forced air cooling of the motor casing [6-9].

Some researchers studied the chimney effect by using numerical simulation method. The chimney effect on smoke spread behavior was revealed with three-dimensional numerical simulations [10]. The results show that the chimney effect significantly influences smoke movement. Natural convection heat transfer and fluid flow in a thermal chimney with multiple horizontally-aligned cylinders was studied by using RANS/URANS simulations for multiple cylinder columns in one or two rows [11]. It was found that the horizontal pitch influences the balance between the chimney effect and the blockage effect, thus has an optimum with respect to the natural draft velocity. The effect of discrete rings and the chimney effect on the enhancement of the natural convection compound heat transfer in a vertical cylinder was studied numerically [12]. Two dissimilar enhancement mechanisms of boundary layer disturbance and flow acceleration obtained by the use of discrete rings and the chimney effect, respectively, were independently analyzed and then combined as one system.

Some researchers studied the chimney effect by using experimental method. The influence of 'chimney-effect' on fire response of rainscreen façades in high-rise buildings was studied by using experimental method [13]. A new experimental setup is developed and demonstrated for the initial screening of façade assembly at a lab-scale. A critical width of the chimney is established at which maximum vertical fire spread was noticed. A new robust hydrogel composite for efficient photothermal interfacial evaporation was developed [14]. The chimney effect was employed to further enhance the water evaporation rate. The chimney effect-induced airflow in a building drainage system in the spread of severe acute respiratory syndrome coronavirus 2 (SARS-CoV-2) was studied [15]. Results showed that the stack air pressure and temperature distributions suggested that stack aerosols can spread to indoors through pipe leaks which provide direct evidence for the long-range aerosol transmission of SARS-CoV-2 through drainage pipes via the chimney effect.

The relevant research developments both domestically and internationally in recent years reveals that the chimney effect indeed affect the fluid flow in varieties of industry areas [10-15]. However, the enhancement of heat transfer for the motor casing by the chimney effect was not studied by now.

At present, the motor casing is not equipped with a heat sink and only relies on the flat or curved surface of the motor casing for heat dissipation, resulting in limited heat dissipation efficiency. In response to this issue, this article developed a motor end cover heat sink and conducted numerical simulation research on the heat dissipation characteristics of three types of heat sinks with or without the chimney effect.

* Corresponding author email: kaiyan@bjtu.edu.cn

2 Structure of air-cooled radiator

Based on the shape characteristics of the motor end cover, this article designs a heat sink and its improved version, which is installed on the motor end cover.

Figure 1 shows the matching diagram between the radiator and the motor, i.e. the motor end cover.

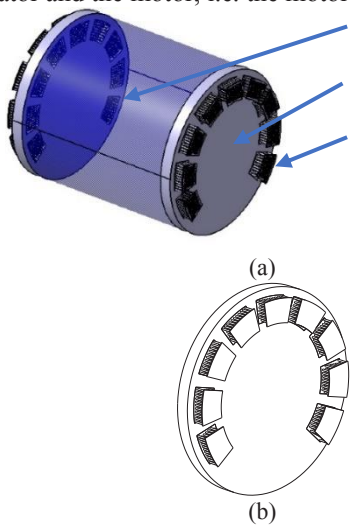

Fig. 1. Schematic diagram of radiator, motor end cover, and motor.

Figure 2 shows a schematic diagram of the radiator and its improved structure.

From Figure 2, it can be seen that Type 1 radiator includes a heat absorbing column, a radiator body, a heat dissipation column, etc; The Type 2 radiator has added a flat heat dissipation cover plate; The heat dissipation cover plate of the Type 3 heat sink has a stamped array convex structure. A semi enclosed structure is formed between the heat dissipation cover plate and the radiator body, which is beneficial for improving the heat dissipation capacity of the radiator under natural heat dissipation conditions based on the chimney effect [9].

In addition, under the condition of forced cooling by traveling wind, adding a heat dissipation cover plate can gather the traveling wind and allow more air to sweep over the heat dissipation column; Moreover, according to the Bernoulli principle, the faster the air flow rate, the lower the pressure, and the increase in the air flow rate around the heat dissipation column, the lower the air pressure around the heat dissipation column, resulting in more air flowing to the heat dissipation column and increasing the air flow rate around the heat dissipation column. This is also beneficial for improving the heat dissipation capacity of the radiator under forced cooling conditions.

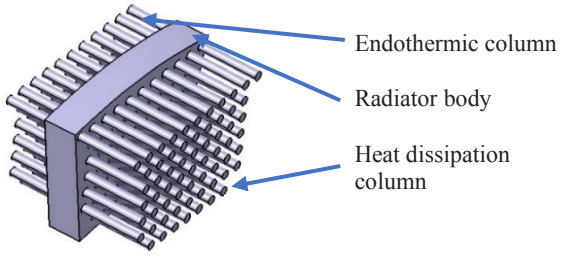

(a) Type 1 radiator

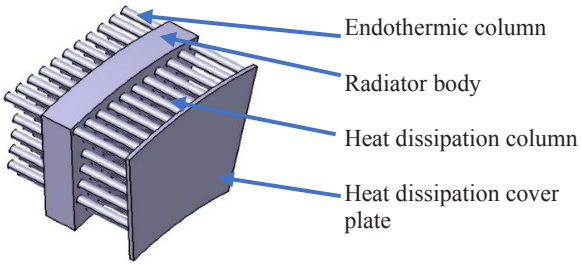

(b) Type 2 radiator

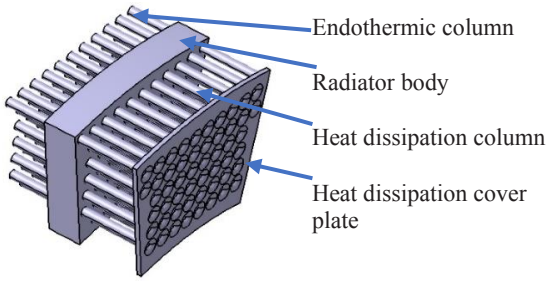

(c) Type 3 radiator

Fig. 2. Structural diagram of radiator and its improved version

3 Numerical simulation calculation method

This article adopts the computational fluid dynamics calculation method to numerically simulate the heat dissipation characteristics of the motor end cover radiator. Air flow usage k- ε Double equation turbulence model.

The following assumptions and simplifications were made in the calculation:

(1) Air flow is an incompressible fluid flow;

(2) Not considering changes in air density caused by temperature changes;

(3) The radiator is a solid of all phases.

Based on this assumption and simplification, establish the fluid continuity equation and momentum equation in vector form in Cartesian coordinate system as follows:

$$\frac{\partial \rho}{\partial t} + div(\rho u) = 0 \quad (1)$$

$$\frac{\partial(\rho u_i)}{\partial t} + div(\rho u_i u) = \frac{\partial(u_{eff} u_i)}{\partial x_i} - \frac{\partial p}{\partial x_i} + S_i \quad (2)$$

$$\frac{\partial(\rho u_j)}{\partial t} + div(\rho u_j u) = \frac{\partial(u_{eff} u_j)}{\partial x_j} - \frac{\partial p}{\partial x_j} + S_j \quad (3)$$

$$\frac{\partial(\rho u_k)}{\partial t} + div(\rho u_k u) = \frac{\partial(u_{eff} u_k)}{\partial x_k} - \frac{\partial p}{\partial x_k} + S_k \quad (4)$$

In equations (1) to (4), ρ is the fluid density, in kg/m^3; t is the time, in seconds; u is the velocity vector, in m/s; p is the pressure, in Pa; x_i 、 x_j 、 x_k are coordinate components; S_i、S_j、S_k are the generalized source term components; μ_{eff} is the effective viscosity coefficient, in Pa·s （$\mu_{eff}=\mu+\mu_t$； μ is the molecular viscosity coefficient, in Pa·s; μ_t is the turbulent viscosity, in N·s/m^2.

The solid structure follows the energy conservation equation:

$$\rho c \frac{\partial T}{\partial t} = \lambda \left(\frac{\partial^2 T}{\partial x^2} + \frac{\partial^2 T}{\partial y^2} + \frac{\partial^2 T}{\partial z^2} \right) \quad (5)$$

In equation (5), x, y, and z are coordinates; ρ is the fluid density in kg/m^3; λ is the thermal conductivity, in W/(m·K); c is the specific heat capacity, in J/(kg·K); t is the time, in seconds; T is the temperature, in K.

Energy equation for air:

$$\frac{\partial(\rho u_i T)}{\partial x_i} = \frac{\partial}{\partial x_i}\left[\left(\frac{\mu}{P_\gamma} + \frac{\mu_t}{\sigma_T}\right)\frac{\partial T}{\partial x_i}\right] + \frac{q_T}{c_p} \qquad (6)$$

In equation (6), μ is the molecular viscosity coefficient, in Pa·s; μ_t is the turbulent viscosity, in N·s/m^2; σ_T is the surface tension, in N/m; q_T is the internal heat source, in W/m^3; c_p is the specific heat capacity at constant pressure, in J/(kg·K).

The initial condition for calculation is that the temperature of each component and air is 40 ℃.

The calculation boundary conditions are:

(1) Under natural cooling conditions, the internal heating power of the motor is 10W;

(2) Under forced air cooling conditions, the running wind speed is 10m/s, and the internal heating power of the motor is 100W.

When the maximum temperature change of the radiator is less than 0.001 ℃, the calculation stops.

4 Calculation results and analysis

This article conducts simulation calculations on the heat dissipation characteristics of radiators under natural cooling conditions and forced air cooling conditions.

Figure 3 shows the distribution of air flow velocity around the heat dissipation column under natural cooling conditions.

From Figure 3, it can be seen that the maximum air flow velocity around the heat dissipation column is 0.095m/s for Type 1 radiator, 0.099m/s for Type 2 radiator, and 0.0992m/s for Type 3 radiator.

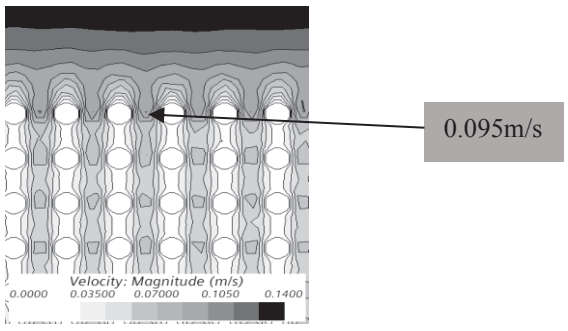

(a) Type 1 radiator

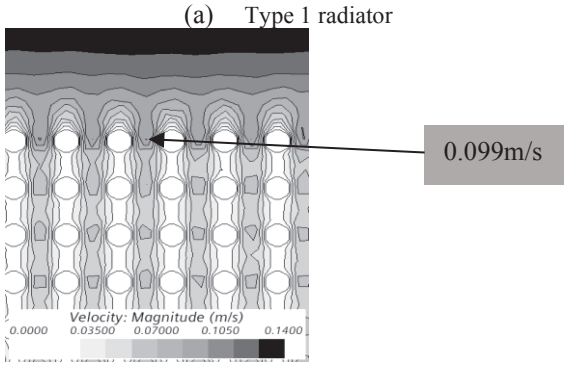

(b) Type 2 radiator

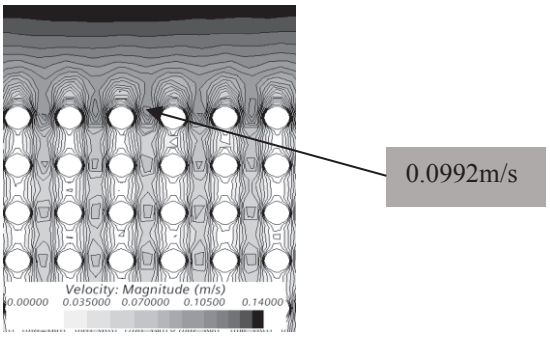

(c) Type 3 radiator

Fig. 3. Distribution of air flow velocity around the heat dissipation column under natural cooling conditions

Figure 4 shows the temperature distribution of the radiator under natural cooling conditions.

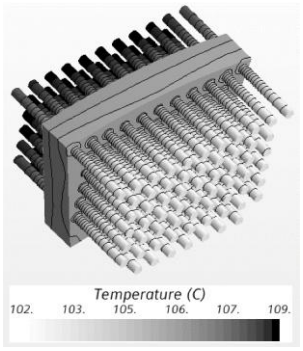

(a) Type 1 radiator

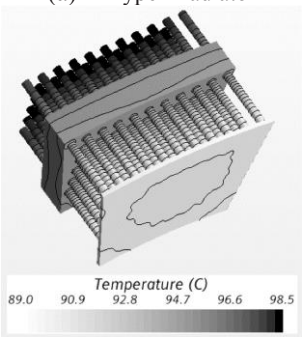

(b) Type 2 radiator

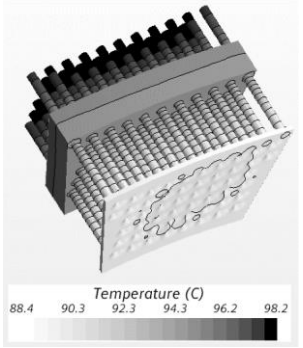

(c) Type 3 radiator

Fig. 4. Temperature distribution diagram of radiator under natural cooling conditions

From Figure 4, it can be seen that the highest temperatures of the heat sink are 109 ℃ for Type 1 heat sink, 98.5 ℃ for Type 2 heat sink, and 98.2 ℃ for Type 3 heat sink.

Figure 5 shows the distribution of air flow velocity and temperature around the radiator under the condition of forced air cooling with running wind.

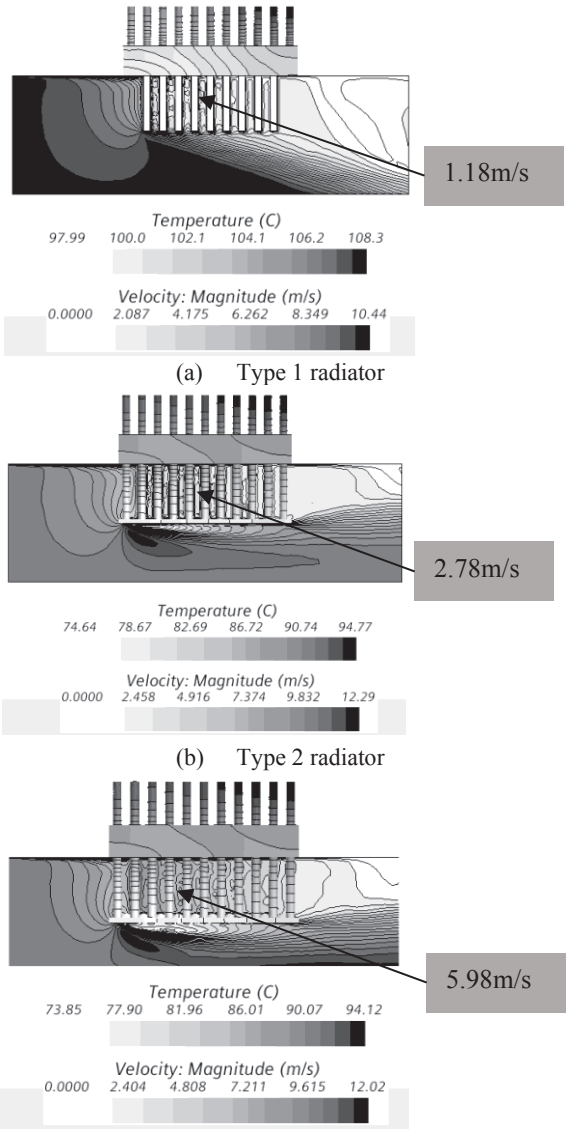

Fig. 5. Distribution of Air Flow Velocity and Radiator Temperature Around the Radiator under Forced Air Cooling Conditions with Traveling Wind

From Figure 5, it can be seen that at the same location, the air flow velocity around the heat dissipation column is 1.18m/s for Type 1 radiator, 2.78m/s for Type 2 radiator, and 5.98m/s for Type 3 radiator, respectively.

From Figure 5, it can also be seen that the highest temperatures of the heat sink are 108.3 ℃ for Type 1 heat sink, 94.7 ℃ for Type 2 heat sink, and 94.1 ℃ for Type 3 heat sink.

5 Conclusion

This article numerically simulates the heat dissipation characteristics of an air-cooled radiator and obtains the following conclusions:

(1) Under natural convection conditions, compared to a heat sink without a heat sink cover (Type 1 heat sink), a heat sink with a flat heat sink cover (Type 2 heat sink) has a 9.6% decrease in maximum temperature, while a heat sink with an array of raised heat sinks cover (Type 3 heat sink) has a 9.9% decrease in maximum temperature.

(2) Under the condition of forced air cooling in the running wind, compared with the heat sink without a heat dissipation cover plate (Type 1 heat sink), the maximum temperature of the heat sink with a flat heat dissipation cover plate (Type 2 heat sink) is reduced by 12.7%, and the maximum temperature of the heat sink with an array raised heat dissipation cover plate (Type 3 heat sink) is reduced by 13.3%.

(3) Under natural cooling conditions, the temperature of the radiator body and heat dissipation column heats the air around the heat dissipation column. Under the action of buoyancy, the air around the heat dissipation column flows upwards, forming a suction effect on the lower temperature air below the radiator, forming a chimney effect and increasing the air flow velocity around the heat dissipation column.

(4) Under forced air cooling conditions, adding a heat dissipation cover plate creates a semi enclosed space between the heat dissipation cover plate and the radiator body, gathering the air flowing around the heat dissipation column and increasing the flow velocity of the air around the cylindrical fins of the radiator. According to Bernoulli's principle, an increase in air flow velocity leads to a decrease in air pressure flowing around the heat dissipation column, which in turn leads to more air flowing towards the heat dissipation column, This increases the amount of forced cooling heat dissipation.

Acknowledgments

The authors acknowledge the support provided by CRRC (2021CYB121, 2022CKB346, 2023CKB343).

References

1. X. Li, *Research on Experiment, Simulation and Application of the Evaporative cooling Heat Exchanger* (Tsinghua University, 2013)
2. Y. Ren, *Dynamic Simulation Study of Pump-Driven Two-Phase Flow Heat Exchange System* (Chongqing University, 2019)
3. X. Sun, *Evaporative Cooling Technology Used for Chip Cooling* (Donghua University, 2011)
4. Z. Li, *Research on Forming and Heat Transfer Performance of Perforated Fin Heat Sink* (Guangdong University of Technology, 2013)
5. B. Chen, G. Gu, Transactions of China Electrotechnical Society **10**, 143-151 (2011)
6. Y. Wei, *Design and optimize on the cooling structure for electric vehicle motor* (Chongqing University of Technology, 2017)
7. X. Lin, *Research on Design and Heat Dissipation for High-Power Servo Motor* (Shenyang University of Technology, 2018)

8. Y. He, et al., *A Natural Heat Dissipation Device Utilizing Chimney Effect* (China patent CN107438349B, 2020
9. A. Muhanmmad, J. China Inst. Water Res. Hydr. Res. **15**, 425-429 (2017)
10. B. Lan, Y. Li, Case Stud. Therm. Eng. **21** (2022)
11. G. Sung, D. Na, S. Yook, Int. J. Heat Mass Tran. **5**, (2022)
12. J. Njoroge, A. Mwaura, Ann. Nucl. Energy, **11** (2022)
13. A. Sharma, K. Mishra, J. Build. Eng. **10** (2021)
14. X. Liang, X. Pei, Desalination, **21** (2022)
15. Q. Wang, Y Li, K. Yuen, J. Hazard. Mater., **2** (2021)